Density functional calculations of the enthalpies of formation of rare-earth orthophosphates†

JAMES R. RUSTAD*

Sullivan Park Research Center, Corning, Inc., Corning, New York 14831, U.S.A.

ABSTRACT

Electronic structure calculations are carried out to estimate the enthalpies of formation of rare-earth orthophosphates from their oxides. The calculated enthalpies of formation are systematically less exothermic than the measured values. The discrepancy is almost entirely in the electronic total energy calculated from density functional theory, and appears to be intrinsic to the generalized-gradient exchange-correlation functional used. However, comparison with electronic structure calculation of the enthalpies of formation of alkaline earth oxyacid carbonates, silicates, and sulfates suggests that near chemical accuracy can be obtained for the enthalpies of formation of most of the compounds in the phosphate system by applying a scaling factor obtained from the simpler alkaline earth oxyacids. The increasingly exothermic ΔH^f_{ox} with increasing ionic radius (i.e., $LaPO_4$ is more exothermic than $ScPO_4$) results from the higher charge localization on the oxide anion (O^{2-}) relative to the phosphate anion (PO_4^{3-}), making it more favorable, in a relative sense, to pair the smaller cation with the oxide anion than with the phosphate anion. This effect is also manifested in ΔH^f_{ox} of the other oxyacids, such as carbonates, silicates, and sulfates.

Keywords: Rare-earth elements, density functional calculations, thermodynamic properties, phosphate minerals

INTRODUCTION

The rare-earth (RE) phosphates are versatile refractory materials with a wide range of geological and technological applications (Ushakov et al. 2002). This paper reports the results of a series of density functional electronic structure calculations of the thermodynamic properties of rare-earth phosphates. The purpose of the paper is to determine how well the calculated enthalpies of formation from the oxides match measured values, and to compare the potential sources of error coming from lattice thermal contributions to the enthalpy, zero-point energies, and electronic energies (the "electronic" energy is the total energy E obtained from the density functional electronic structure calculation at 0 K). Another aim of the paper is to obtain a more fundamental understanding why the enthalpies of formation of these compounds from the oxides are more exothermic for the larger rare earth elements.

This information is important for several reasons. First, studies of a systematic series of minerals (Jain et al. 2011) can be an important component of developing better density functionals for thermal properties. Second, studies of interfacial properties of these minerals, in contact with both aqueous and silicate solvents, will require construction of potential functions (Pedone et al. 2006). Although it is common to use structural and elastic properties to construct empirical potential functions, energetics of reactions such enthalpies of formation from the oxides ΔH^f_{ox} (298.15 K) (e.g., $\frac{1}{2}Ln_2O_3 + \frac{1}{2}P_2O_5 = LnPO_4$) are often not considered. Tables of electronic enthalpies of forma-

tion at 0 K, if available (and accurate, of course) would aid in the construction of transferable potential functions, which may eventually be capable of predicting thermodynamic properties of complex mixtures, such as glasses and melts. It is hoped that input on formation energies from first-principles methods will facilitate these efforts.

METHODS

Electronic structure calculations are carried out with density functional theory (DFT) using the projector augmented wave (PAW) method (Bloechl 1994) implemented in VASP 4.6.11 (Kresse and Furthmuller 1996; Kresse and Hafner 1993), with PAW pseudopotentials (Kresse and Joubert 1999) constructed for the PBE exchange correlation functional (Perdew et al. 1996). The calculations on the lanthanide elements use the Ln_3 trivalent lanthanide pseudopotentials. These provide an implicit treatment of the f electron shell across the series of rare earth elements. Calculations for yttrium and scandium use the Y_sv and Sc_sv pseudopotentials. $LuPO_4$ failed to achieve SCF convergence, so this was eliminated from the study, along with Pm (no experimental data) as well as Eu and Yb, due to the lack of Eu_3 and Yb_3 PAW pseudopotentials. DFT+U calculations are carried out for Ce_2O_3 and $CePO_4$ using the standard Ce PBE pseudopotential and a U value of 3 eV, which was found to be an optimal value both for Ce_2O_3 (Fabris et al. 2005; Loschen et al. 2007) and $CePO_4$ (Adelstein et al. 2011). The DFT+U calculations use the method of Dudarev et al. (1998).

The cutoff energy was set to 500 eV for all systems. A γ-centered reciprocal space grid was used for each system. The following **k**-point grid sizes were used: For the C-oxide, monazite, and xenotime structures, $7 \times 7 \times 7$; for the A-oxide structures, $15 \times 15 \times 15$; for h-P_4O_{10} and o'-P_2O_5, $7 \times 7 \times 7$. Structure optimizations were done with both volume and lattice vectors varying simultaneously. Final structures were run with no optimization to ensure that the absolute value of the pressure was below 0.1 GPa. Final configurations outside this range were optimized again until the pressure criterion was satisfied.

RESULTS AND DISCUSSION

Structure and energetics of RE_2O_3 oxides

Tables 1, 2, and 3 give the optimized structural parameters and molar volume for the A-, B-, and C-type RE_2O_3 oxides,

TABLE 1. Structural parameters for hexagonal A-type RE_2O_3 (volumes in Å³/formula unit)

| | Calculated | | | | | | | | | Measured | | |
| | This work | | | Hirosaki et al. (2003) | | | Wu et al. (2007) | | | | | |
	a (Å)	c (Å)	V (Å³)	a (Å)	c (Å)	V (Å³)	a (Å)	c (Å)	V (Å³)	a (Å)	c (Å)	V (Å³)
La_2O_3*	3.936	6.200	83.20	3.936	6.166	82.73	3.938	6.173	82.90	3.940	6.13	82.410
Ce_2O_3†	3.944	6.180	83.26	3.941	6.182	83.14	3.944	6.191	83.38	3.891	6.059	79.440
Ce_2O_3 (PBE+U) AFM	3.897	6.229	81.91									
Ce_2O_3 (PBE+U) FM	3.892	6.224	81.66									
Pr_2O_3‡	3.896	6.135	80.64	3.895	6.126	80.50	3.899	6.135	80.76	3.859	6.0131	77.550
Nd_2O_3§	3.867	6.082	78.77	3.859	6.072	78.30	3.859	6.090	78.54	3.831	5.999	76.250

* Koehler and Wollan (1953).
† Schiller (1985).
‡ Hase (1963).
§ Boucherle and Schweizer (1975).

TABLE 2. Structural parameters for monoclinic B-type RE_2O_3 (volume in Å³/formula unit)

	a (Å)	b (Å)	c (Å)	β	V (Å³)
	calc (this work)				
Sm_2O_3	14.384	3.631	8.916	100.26	76.36
Gd_2O_3	14.177	3.565	8.770	100.30	72.68
	calc*				
Sm_2O_3	14.381	3.635	8.911	100.15	76.41
Gd_2O_3	14.195	3.566	8.770	100.18	72.80
	measured				
Sm_2O_3†	14.198	3.627	8.856	99.99	74.66
Gd_2O_3‡	14.032	3.583	8.742	100.13	72.11

* Wu et al. (2007).
† Boulestix et al. (1971).
‡ Zhang et al. (2008a).

TABLE 3. Structural parameters for cubic C-type RE_2O_3 (volume in Å³/formula unit)

| | Calculated | | | | Measured | |
| | This work | | Hirosaki et al. (2003) | | | |
	a (Å)	V (Å³)	a (Å)	V (Å³)	a (Å)	V (Å³)
Sc_2O_3	9.911	60.85			9.846*	59.66
Y_2O_3	10.701	76.58			10.596†	74.36
La_2O_3	11.387	92.29	11.392	92.40		
Ce_2O_3	11.414	92.94	11.410	92.84	11.111‡	85.73
Pr_2O_3	11.290	89.94	11.288	89.89		
Nd_2O_3	11.178	87.30	11.176	87.24		
Sm_2O_3	10.998	83.14	10.995	83.07	10.930§	81.61
Gd_2O_3	10.819	79.16	10.812	78.99	10.790§	78.51
Tb_2O_3	10.744	77.50			10.729‖	77.10
Dy_2O_3	10.675	76.02	10.670	75.92	10.670§	75.92
Ho_2O_3	10.609	74.63	10.605	74.54	10.580§	74.02
Er_2O_3	10.544	73.26	10.544	73.26	10.548#	73.35
Tm_2O_3	10.472	71.77			10.480**	71.94

* Knop and Hartley (1963).
† Baldinozzi et al. (1998).
‡ Kuemmerle and Heger (1999).
§ Bartos et al. (1993).
‖ Saiki et al. (1985).
Fert (1962).
** Hase (1963).

respectively, along with values obtained from X-ray measurements (Koehler and Wollan 1953; Fert 1962; Hase 1963; Knop and Hartley 1968; Boulesteix et al. 1971; Boucherle and Schweizer 1975; Saiki et al. 1985; Schiller 1985; Bartos et al. 1993; Greis et al. 1994; Baldinozzi et al. 1998; Kuemmerle and Heger 1999; Zhang et al. 2008). The large RE oxides La_2O_3, Ce_2O_3, Nd_2O_3, and Pr_2O_3 are known to be most stable in the hexagonal A-type structure. Previous work (Wu et al. 2007) compared the electronic energies of a series of rare-earth oxides in the A-type and monoclinic B-type structure using the same method used here (PAW-PBE), but did not report results for the cubic C-type structure. An earlier PAW-GGA study

(Hirosaki et al. 2003) gave structures but not energies for the C-type oxides. Table 4 gives the calculated energies for the suite of RE oxide compounds in the C-type structure as well as the A-type structure for La, Ce, Nd, and Pr, and the B-type structure for Sm and Gd. The results are very close to those previously calculated. The results show that PAW-PBE predicts (incorrectly) that La, Ce, Nd, Pr, and Sm are most stable in the C-type structure. This was already noted for Ce_2O_3 (Da Silva 2007). As shown in Tables 1–3, calculated molar volumes are generally 2–3% greater than measured values, except for A-Ce_2O_3, which is 4.8% above the measured value. This finding is consistent with the general tendency of functionals in the generalized gradient approximation to overestimate bond lengths. The PAW PBE+U calculations give improved calculations of the volume and lattice parameters for the A-Ce_2O_3 (this study; Da Silva 2007) and C-Ce_2O_3 (Da Silva 2007) phases. They are also reported to stabilize A-type Ce_2O_3 over C-type Ce_2O_3 (Da Silva 2007) (DFT+U calculations were not done on C-Ce_2O_3 in the present study).

Structures and energetics of $REPO_4$ phosphates

Tables 5 (xenotime) and 6 (monazite) give the optimized structural parameters for the RE orthophosphates. Comparisons are made with the X-ray measurements (Ni et al. 1995; Milligan et al. 1982). The data overestimate volumes by close to 2% for the monazite-type $REPO_4$, and 2–3% for the xenotime $REPO_4$, except for $CePO_4$(m), which is overestimated by 4.6% with PBE and Ce_3 pseudopotential. The structure is improved slightly in the PBE+U treatment. The structural calculations are in line with those of the oxides.

Calculated electronic energies for the $REPO_4$ are given in Table 7. Lanthanum, Ce, Pr, and Nd are all most stable in the monazite structure, in agreement with observations (although actual measured values for ΔG^f_{ox} of the monazite-xenotime polymorphs are not available for any of the $REPO_4$). For $NdPO_4$, the monazite and xenotime structures are nearly isoenergetic. For Tb-Tm, as well as Sc and Y, the xenotime structure is most stable, also in line with observations. $SmPO_4$ and $GdPO_4$ are also calculated to be more stable in the xenotime structure. The PBE+U calculations on $CePO_4$ give a low-energy antiferromagnetic structure almost isoenergetic with the ferromagnetic solution. The PBE+U treatment increases the stabilization of FM-$CePO_4$(m) relative to FM-$CePO_4$(x) by about 20 kJ/mol [searches for AFM structures were not carried out for $CePO_4$(x) in the present study].

TABLE 4. Energies of RE_2O_3 phases (eV/formula unit)

	C-type	A-type	B-type	A-type*	B-type*
Sc_2O_3	−45.2887			−44.6351	−44.9478
Y_2O_3	−45.5652			−45.2299	−45.3291
La_2O_3	−42.0219	−41.9007		−41.9079	−41.8576
Ce_2O_3	−40.7455	−40.6337		−40.6376	−40.6027
Ce_2O_3 (PBE+U) AFM		−41.6814			
Ce_2O_3 (PBE+U) FM		−41.6791			
Pr_2O_3	−41.0188	−40.8856		−40.8945	−40.8744
Nd_2O_3	−41.2258	−41.0714		−41.0803	−41.0746
Sm_2O_3	−41.5301		−41.3677	−41.3363	−41.362
Gd_2O_3	−41.8636		−41.6746	−41.6172	−41.6718
Tb_2O_3	−41.9675			−41.7017	−41.7655
Dy_2O_3	−42.0428			−41.7398	−41.8283
Ho_2O_3	−42.1142			−41.8004	−41.8883
Er_2O_3	−42.2007			−41.8377	−41.9627
Tm_2O_3	−42.1943			−41.7963	−41.9437

* Wu et al. (2007).

TABLE 5. Structural parameters for $REPO_4$ in the xenotime (zircon) structure (volume in Å³/formula unit)

	Calculated			Measured		
	a (Å)	c (Å)	V (Å³)	a (Å)	c (Å)	V (Å³)
$ScPO_4$*	6.661	5.837	64.740	6.574	5.791	62.568
YPO_4*	6.976	6.079	73.950	6.895	6.028	71.633
$TbPO_4$†	6.984	6.086	74.205	6.931	6.061	72.784
$DyPO_4$†	6.953	6.066	73.328	6.905	6.038	71.981
$HoPO_4$†	6.934	6.050	72.710	6.877	6.018	71.154
$ErPO_4$†	6.905	6.026	71.823	6.851	5.997	70.363
$TmPO_4$†	6.880	5.998	70.968	6.829	5.980	69.726
$LaPO_4$	7.274	6.347	83.945			
$CePO_4$	7.261	6.342	83.575			
$CePO_4$ (PBE+U‡)	7.233	6.314	82.62			
$PrPO_4$	7.209	6.293	81.768			
$NdPO_4$	7.178	6.247	80.473			
$SmPO_4$	7.089	6.187	77.728			
$GdPO_4$	7.015	6.116	75.248			

* Milligan et al. (1982).
† Ni et al. (1995).
‡ Ferromagnetic electronic state.

TABLE 6. Structural parameters for $REPO_4$ in the monazite structure (volume in Å³/formula unit)

	Calculated					Measured*				
	a (Å)	b (Å)	c (Å)	β (°)	V (Å³)	a (Å)	b (Å)	c (Å)	β (°)	V (Å³)
$LaPO_4$	6.932	7.142	6.543	103.6	78.71	6.831	7.071	6.503	103.3	76.43
$CePO_4$	6.916	7.135	6.535	103.5	78.40	6.788	7.016	6.465	103.4	74.98
AFM1†	6.900	7.110	6.510	103.5	77.62					
AFM2	6.883	7.099	6.522	103.5	77.44					
AFM3	6.908	7.113	6.515	103.5	77.82					
FM‡	6.899	7.105	6.518	103.6	77.64					
$PrPO_4$	6.873	7.079	6.485	103.8	76.61	6.760	6.981	6.434	103.5	73.80
$NdPO_4$	6.840	7.040	6.452	103.8	75.42	6.735	6.950	6.405	103.7	72.83
$SmPO_4$	6.803	6.961	6.394	104.2	73.38	6.682	6.888	6.365	103.9	71.10
$GdPO_4$	6.713	6.887	6.358	104.2	71.24	6.644	6.841	6.328	104.0	69.78
$TbPO_4$	6.687	6.858	6.337	104.2	70.42					

* Ni et al. (1995).
† Antiferromagnetic electronic states for PBE+U.
‡ Ferromagnetic electronic state for PBE+U.

TABLE 7. Calculated energies of $REPO_4$ (eV/formula unit)

	x-type	m-type
$ScPO_4$(x)	−48.845	
YPO_4(x)	−49.760	
$LaPO_4$(m)	−48.215	−48.337
$CePO_4$(m)	−47.679	−47.805
$CePO_4$ (PBE+U) AFM1		−48.280
$CePO_4$ (PBE+U) AFM2		−48.304
$CePO_4$ (PBE+U) AFM3		−48.251
$CePO_4$ (PBE+U) FM	−47.970	−48.302
$PrPO_4$(m)	−47.779	−47.843
$NdPO_4$(m)	−47.846	−47.854
$SmPO_4$(m)	−47.923	−47.835
$GdPO_4$(m)	−48.013	−47.819
$TbPO_4$(x)	−48.027	−47.788
$DyPO_4$(x)	−48.025	
$HoPO_4$(x)	−48.022	
$ErPO_4$(x)	−48.031	
$TmPO_4$(x)	−47.991	

Structures and energetics of P_2O_5

For calculation of the electronic energies of formation from the oxides, the total energy of the P_2O_5 reference phase is needed. In the study of Ushakov et al. (2002), the reference phase was the hexagonal h-P_2O_5. This is a molecular solid having discrete adamantane-like P_4O_{10} molecules held together by van der Waals interactions that are not accounted for in the DFT. The omission of this contribution to the cohesive energy of P_2O_5 will produce a systematic error in the calculations, with the calculated ΔE_{ox}^r being consistently too negative. It is known that the h-P_2O_5 phase is metastable with respect to a polymeric (i.e., non-molecular) orthorhombic o'-P_2O_5 compound (Greenwood and Earnshaw 1985) in which molecular Van der Waals forces presumably play a much smaller role in the bonding. As an upper bound to the required correction, it could be assumed that the total energies of h-P_2O_5 and o'-P_2O_5 are equal and the total energy of o'-P_2O_5 could be used as a surrogate for h-P_2O_5. The structural parameters and energies of both phases are given in Table 8 and compared with X-ray measurements (Cruickshank 1964; Stachel et al. 1995). The calculated electronic energy of o'-P_2O_5 is 14.84 kJ/mol lower than h-P_2O_5. Here, all calculations are reported relative to h-P_2O_5.

Formation of $REPO_4$ from RE_2O_3 and P_2O_5

Table 9 shows the electronic energies at 0 K [$\Delta E_{ox}^r(0) = E(REPO_4) − \frac{1}{2}(E(P_2O_5) + E(RE_2O_3))$] for the reaction:

$$\tfrac{1}{2}P_2O_5 + \tfrac{1}{2}RE_2O_3 = REPO_4$$

and compared with the measured enthalpies of formation from the oxides at 298.15 K from Ushakov et al. (2002). Figure 1 shows the correlation between $\Delta H_{ox}^r(298.15)$ and the ionic radius of the RE cation noted by Ushakov et al. (2002), with the cube root of calculated molar volume of the cubic oxide serving as a convenient surrogate for the "computed" value of the ionic radius of the RE cation (this is simpler than, for example, trying to average the calculated RE-O distances). $GdPO_4$, in the monazite structure, deviates most strongly from the correlation. $GdPO_4$ shows no anomalous predictions in the structural properties of either the RE_2O_3 or $REPO_4$ phases, and does not deviate strongly in the experimental correlation [Fig. 3 in Ushakov et al. (2002)] so the reasons for the large deviation from the energy vs. size correlation are not clear, except to note that using the xenotime polymorph for $GdPO_4$(x), which is, incorrectly, calculated to be lower in energy than $GdPO_4$(m), lies much closer to the correlation than $GdPO_4$(m). $TbPO_4$(m) also lies off the correlation, however, in the case of terbium, $TbPO_4$(x) is, correctly, calculated to lower in energy than $TbPO_4$(m), and falls close to the main trend. There is an indication of a separate, steeper trend for the monazite structures than the xenotime structures. Such a difference was not apparent on the experimental correlation; $\Delta H_{ox}^r(298.15)$ for $TbPO_4$(x) and $TbPO_4$(m) were measured within 3 kJ/mol of each other. This can

TABLE 8. Structural parameters and energies of P_2O_5 phases

	(a,b,c) (Å)	(α,β,γ) °		V (Å³)	E (eV/formula unit)
h-P_2O_5	7.592	87.6		109.1	−48.9743
measured*	7.43	87		102.1	
	a (Å)	b (Å)	c (Å)		
o'-P_2O_5	9.534	4.952	7.308	345.0	−49.1281
measured†	9.139	4.89	7.162	320.1	

* Cruickshank (1964).
† Stachel et al. (1995).

TABLE 9. Measured vs. calculated electronic energy

	$\Delta H^f_{ox}(298.15)$ kJ/mol*	$\Delta E^f_{ox}(0)$ kJ/mol	$\Delta E^f_{ox}(0)$ kJ/mol MGP	$\Delta E^f_{ox}(0)$ MGP/ $\Delta H^f_{ox}(298.15)$	$\Delta H^f_{ox}(298.15) -$ [$\Delta E^f_{ox}(0)$ MGP/0.85]) kJ/mol
$YPO_4(x)$	−282.6	−240.2	−236	0.84	−5.0
$LaPO_4(m)$	−321.4	−279.7	−270	0.84	−3.8
$LaPO_4(x)$		−268.0			
$CePO_4(m)$	−317.2	−289.6	−241†		
PBE+U AFM1		−287.1			
PBE+U AFM2		−284.8			
PBE+U AFM3		−282.0			
PBE+U FM		−287.0			
$CePO_4(x)$		−277.4			
$PrPO_4(m)$	−312.2	−281.1	−271	0.87	6.6
$PrPO_4(x)$		−274.8			
$NdPO_4(m)$	−312.0	−273.2	−262	0.84	−3.8
$NdPO_4(x)$		−272.3			
$SmPO_4(m)$	−301.8	−257.1	−245	0.81	−13.6
$SmPO_4(x)$		−265.5			
$GdPO_4(m)$	−296.2	−231.6	−236†		
$GdPO_4(x)$		−250.3			
$TbPO_4(x)$	−286.1	−246.6	−243	0.85	−0.4
$TbPO_4(m)$	−283.5	−223.5			
$DyPO_4(x)$	−283.9	−242.8	−239	0.84	−2.7
$HoPO_4(x)$	−278.8	−239.1	−235	0.84	−2.3
$ErPO_4(x)$	−275.6	−235.7	−232	0.84	−2.7
$TmPO_4(x)$	−268.0	−232.2	−228	0.85	0.2
$ScPO_4(x)$	−209.8	−165.4	−161	0.77	−20.4
$LuPO_4$	−263.9		−220	0.83	−5.2
$YbPO_4$	−269.6		−252†		

* Ushakov et al. (2002).
† Calculation not done with Ln_3 pseudopotential in MGP.

$\sqrt[3]{V_{ox}}$ (Å)
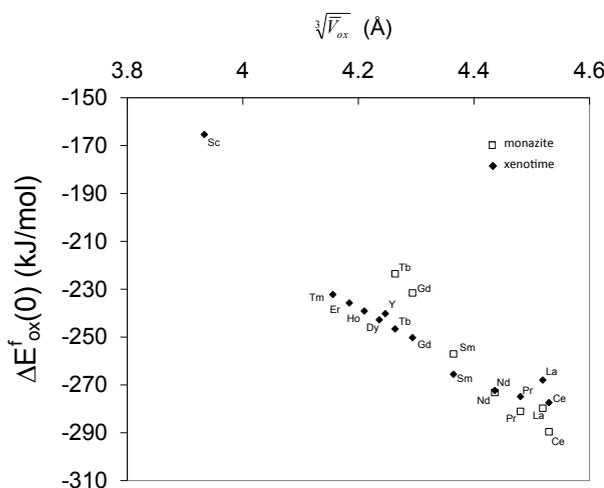
FIGURE 1. Correlation between $\Delta E^f_{ox}(0)$ and the cube root of the computed volume of the RE_2O_3 phase for monozite and xenotime.

be compared against the 23 kJ/mol difference in $\Delta E^f_{ox}(0)$ for these phases; so it can be concluded that the DFT calculations overestimate the energetic differences between the two polymorphs.

$\sqrt[3]{V_{ox}}$ (Å)
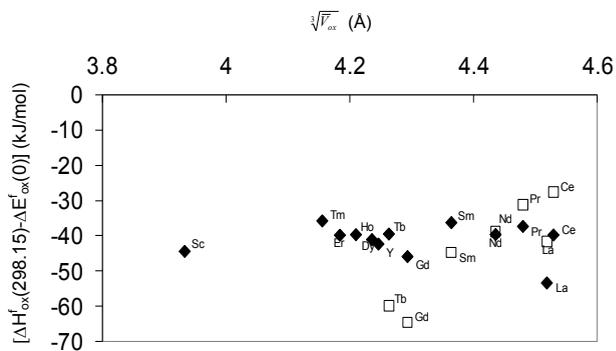
FIGURE 2. Correlation between the difference of the measured heat of formation and the computed electronic energy [$\Delta H^f_{ox}(298.15) - \Delta E^f_{ox}(0)$] and the cube root of the computed volume of the cubic RE_2O.

Figure 2 shows $\Delta H^f_{ox}(298.15)$-$\Delta E^f_{ox}(0)$ plotted again against the cube root of the volume of the cubic RE_2O_3 phase. The measured $\Delta H^f_{ox}(298.15)$ values lie fairly consistently about 40 kJ/mol lower than the calculated $\Delta E^f_{ox}(0)$, and exhibit no convincing trend with ionic radius. The average deviation would be increased to ~50 kJ/mol if o'-P_2O_5 were used instead of h-P_2O_5 as the P_2O_5 reference compound. The most negative deviations from the average (i.e., the $REPO_4$ phase is calculated to be thermodynamically less stable than average) occurs for $GdPO_4$ and $TbPO_4$. The most positive deviation is for $CePO_4$. Unlike $GdPO_4$, calculated structural properties of $CePO_4$ are anomalous. The predicted volume of $CePO_4$ is nearly 4.6% above X-ray measurements, in contrast to the 2–3% for the other $REPO_4$. The overestimation of the volume is 4.8% for the Ce_2O_3. Treatment of $CePO_4$ and Ce_2O_3 with PBE+U makes only a small correction (~3 kJ/mol) to the calculated $\Delta E^f_{ox}(0)$, so the effective RE_3 pseudopotentials are probably not the source of the error shown in Figure 2. The data in Figure 2 may suggest that the monazite $REPO_4(m)$ phases lie on a different trend than the xenotime $REPO_4(x)$ phases.

Thermal corrections to $\Delta E^f_{ox}(0)$

Direct comparison of the calculated $\Delta E^f_{ox}(0)$ for the formation of the $REPO_4$ from oxides with experimental $\Delta H(298 K)$ requires, at a minimum, knowledge of the differential zero-point energies $\Delta ZPE = ZPE(LnPO_4) - 1/2[ZPE(P_2O_5) + ZPE(Ln_2O_3)]$ and the differential enthalpies $\Delta\int C_P dT = \int\{C_P(LnPO_4) - 1/2[C_P(Ln_2O_3) + C_P(P_2O_5)]dT\}$ between $(P_2O_5+Ln_2O_3)$ and $LnPO_4$. These could, in principle, be computed from DFT for all phases, but would require a heavy investment of computational resources. Here, an empirical approach is taken to estimate the likely magnitude of the thermal contributions. There will also be Schottky-type contributions for some of the phases (Westrum 1985), but these cannot be responsible for the systematic differential between the measured and calculated enthalpies, as they should be close to zero for compounds with no crystal-field stabilization (Y, Sc, La, Gd).

The $\Delta\int C_P dT$ can be summed from low-temperature heat capacities of the RE_2O_3, P_2O_5, and $REPO_4$ phases. Low-temperature heat capacities for the RE_2O_3 phases (Goldstein et al. 1959; Justice and Westrum 1963; Weller and King 1963; Justice et al. 1969; Gavrichev et al. 1993; Gruber et al. 2002) are given in

Table 10. For the REPO$_4$ phases, low-temperature heat capacities have been measured for ScPO$_4$ (Gavrichev et al. 2010a), YPO$_4$ (Gavrichev et al. 2010b), LaPO$_4$ (Gavrichev et al. 2008), and LuPO$_4$ (Gavrichev et al. 2006). The low-temperature heat capacity of P$_2$O$_5$ has been measured by Andon et al. (1963) giving $H(298.15) – H(0) = 16.98$ kJ/mol; first-principles electronic structure calculations yield estimates of $H(298.15)–H(0) = 16.37$ kJ/mol (Rustad 2011). Taking typical values of ~20 kJ/mol for RE$_2$O$_3$, ~17 kJ/mol for REPO$_4$, and ~16 kJ/mol for P$_2$O$_5$, the thermal enthalpy correction to $\Delta E_{ox}^r(0)$ is close to zero (–1 kJ/mol), and, as expected, make negligible contribution to the systematic difference between $\Delta H_{ox}^r(298\,K)$ and $\Delta E_{ox}^r(0)$.

Estimates for ZPEs can be made empirically from knowledge of the infrared and Raman vibrational spectra for each of the phases. Uncertainties related to the deconvolution of multicomponent peaks, knowledge of vibrational degeneracies, and anharmonic effects contribute to inaccuracies in these estimates.

A normal coordinate analysis has been carried for A-type (La-Pr-Nd)$_2$O$_3$ (Gopinath and Brown 1982). Infrared and Raman spectra have been measured for LnPO$_4$ (Ln = La, Ce, Pr, Nd, Sm, Eu, Gd) (Silva et al. 2006). Infrared and Raman spectra have been obtained for h-P$_4$O$_{10}$ (Gilliam et al. 2003), however the ZPE for P$_2$O$_5$ (70.6 kJ/mol) is taken from a recent theoretical calculation of the vibrational spectrum of this phase (Rustad 2011) because of some revisions in the interpretation of the measured spectrum indicated by the calculations. The vibrational frequencies and ZPE estimates are given in Tables 11 and 12. Again, taking typical values, an estimate for ΔZPE is 58 kJ/mol – ½(21.5 – 70.6). This yields a +12 kJ/mol correction to the calculated $\Delta E_{ox}^r(0)$, in the opposite direction of the correction needed to bring the calculated $\Delta E_{ox}^r(0)$ in consonance with measured values of $\Delta H(298\,K)$; in other words, the calculated enthalpies, which are already not exothermic enough, become ~12 kJ/mol *less* exothermic by accounting for the ZPE.

To check these estimates, first-principles calculations of the vibrational spectrum of YPO$_4$ and cubic Y$_2$O$_3$ were carried out using the CASTEP planewave-pseudopotential code (Clark et al. 2005), as implemented within Materials Studio of Accelrys, Inc. A planewave cutoff of 750 eV and norm-conserving pseudopotentials (Lin et al. 1993) were used in the calculations. The phonons were calculated with the linear-response method (Refson et al. 2006). For Y$_2$O$_3$ and YPO$_4$ the norm-conserving pseudopotentials give structures that compare well with the VASP calculations and

TABLE 10. Enthalpy correction to standard temperature $H(298.15) – H(0)$ for RE$_2$O$_3$ phases (kJ/mol)

	RE$_2$O$_3$	REPO$_4$
Sc	13.845*	14.934**
Y	16.800†	15.944††
La	19.842‡	17.440‡‡
Ce	21.479‡	
Pr	22.734‡	
Nd	20.892‡	
Sm	21.008§	
Gd	18.510§	
Dy	21.025‖	
Ho	20.958‖	
Er	19.995‖	
Tm	20.887#	
Lu	17.539#	16.430§§

* Weller and King (1963).
† Gavrichev et al. (1993).
‡ Gruber et al. (2002).
§ Justice and Westrum (1963).
‖ Westrum and Justice (1963).
Justice et al. (1969).
** Gavrichev et al. (2010a).
†† Gavrichev et al. (2010b).
‡‡ Gavrichev et al. (2008).
§§ Gavrichev et al. (2006).

TABLE 12. Vibrational frequencies (cm^{-1}) with hν/2 contribution to zero-point energy (kJ/mol) for A-type Ln$_2$O$_3$ oxide phases*

	La$_2$O$_3$		Pr$_2$O$_3$		Nd$_2$O$_3$	
E$_g$	413	4.9	415	5.0	434	5.2
A$_{1g}$	400	2.4	404	2.4	422	2.5
E$_u$	408	4.9	409	4.9	415	5.0
A$_{2a}$	404	2.4	406	2.4	407	2.4
E$_u$	243	2.9	264	3.2	232	2.8
A$_{2u}$	256	1.5	258	1.5	223	1.3
A$_{1g}$	191	1.1	189	1.1	190	1.1
E$_g$	99	1.2	99	1.2	100	1.2
		21.4†		21.7†		21.6†

* Data taken from Gopinath and Brown (1982).
† Total zero-point energy (Σhν_i/2).

TABLE 11. Vibrational frequencies (cm^{-1}) with hν/2 contribution to zero-point energy (kJ/mol) for monazite-type LnPO$_4$*

LaPO$_4$		CePO$_4$		PrPO$_4$		NdPO$_4$		SmPO$_4$		EuPO$_4$		GdPO$_4$	
90	0.5	88	0.5	90	0.5	89	0.5	88	0.5	87	0.5	87	0.5
100	0.6	100	0.6	105	0.6	106	0.6	107	0.6	108	0.6	108	0.6
151	0.9	152	0.9	153	0.9	154	0.9	155	0.9	156	0.9	158	0.9
157	0.9	158	0.9	160	1.0	160	1.0	159	1.0	160	1.0	162	1.0
170	1.0	172	1.0	176	1.1	175	1.0	177	1.1	175	1.0	178	1.1
184	1.1	183	1.1	182	1.1	183	1.1	185	1.1	189	1.1	192	1.1
219	1.3	219	1.3	225	1.3	228	1.4	231	1.4	234	1.4	236	1.4
226	1.4	227	1.4	233	1.4	236	1.4	243	1.5	243	1.5	247	1.5
258	1.5	254	1.5	260	1.6	264	1.6	265	1.6	265	1.6	268	1.6
275	3.3	270	1.6	282	1.7	291	1.7	293	1.8	298	1.8	302	1.8
396	2.4	396	2.4	299	1.8	398	2.4	404	2.4	404	2.4	406	2.4
413	2.5	414	2.5	417	5.0	419	2.5	424	2.5	425	2.5	428	2.6
466†	5.6	467	5.6	470	5.6	471	5.6	474	5.7	472	5.6	478	5.7
620‡	11.1	618	11.1	623	11.2	625	11.2	629	11.3	631	11.3	634	11.4
968§	5.8	970	5.8	975	5.8	977	5.8	983	5.9	990	5.9	988	5.9
1054‖	18.9	1054	18.9	1058	19.0	1061	19.0	1065	19.1	1069	19.2	1072	19.2
	58.8#		57.1#		59.6#		57.9#		58.3#		58.5#		58.8#

* Data taken from Silva et al. (2006).
† PO$_4$-ν_2 (multiplicity 2).
‡ PO$_4$-ν_4 (multiplicity 3).
§ PO$_4$-ν_1 (multiplicity 1).
‖ PO$_4$-ν_3 (multiplicity 3).
Total zero-point energy (Σhν_i/2).

TABLE 13. Thermodynamic properties obtained with CASTEP

	E	ZPE (kJ/mol)	C_V [J/(mol·K)]	$H(298.15) - H(0)$ (kJ/mol)	$S(298.15)$ [J/(mol·K)]
YPO$_4$ calc (this work)	–1957.54 eV	53.14	96.84 (C_V)	15.001	87.28
exp*		–	99.27 (C_P)	15.994	93.86
Y$_2$O$_3$ calc (this work)	–1393.97 eV	33.45	93.66	14.760	85.92
exp†		–	103.4	16.800	98.96
h-P$_2$O$_5$ calc‡	–2516.15 eV	70.65	103.1	16.370	106.45
$\Delta E_{ox}^f(0)$	–239.28 kJ/mol				
Correction to H calc		1.09			–0.56
exp§	–282.6 kJ/mol				–0.59

* Gavrichev et al. (2010).
† Gavrichev et al. (1993).
‡ Rustad (2011).
§ Ushakov et al. (2002).

TABLE 14. Computed vibrational modes at q = (0,0,0) for Y$_2$O$_3$

ν (cm⁻¹)	g*	IR Int†	R‡	RM§
114.4	1	0.00	N	N
122.0	3	0.04	Y	N
132.1	3	0.00	N	Y
135.7	2	0.00	N	N
141.1	3	0.00	N	Y
159.0	3	0.01	Y	N
166.6	1	0.00	N	Y
177.2	3	0.23	Y	N
187.5	3	0.17	Y	N
193.0	3	0.00	N	Y
207.1	2	0.00	N	Y
207.9	3	0.06	Y	N
241.7	1	0.00	N	N
253.2	3	0.00	N	Y
257.3	3	0.00	N	Y
260.7	2	0.00	N	N
261.6	3	1.08	Y	N
320.2	3	0.00	Y	N
378.6	3	88.12	Y	N
385.1	3	0.00	N	Y
393.5	3	2.04	Y	N
394.9	1	0.00	N	N
397.1	2	0.00	N	Y
398.5	3	0.00	N	Y
412.5	3	51.24	Y	N
419.7	1	0.00	N	Y
420.6	2	0.00	N	N
425.5	3	1.70	Y	N
435.1	3	0.00	N	Y
448.6	3	100.11	Y	N
452.3	3	0.00	N	Y
463.4	2	0.00	N	Y
470.6	2	0.00	N	N
471.6	3	0.00	N	Y
476.5	3	3.71	Y	N
506.0	1	0.00	N	Y
514.7	3	0.00	N	Y
518.5	1	0.00	N	N
551.8	3	4.12	Y	N
556.5	3	0.00	N	Y
580.4	1	0.00	N	N
581.4	3	0.02	Y	N
593.1	3	0.00	N	Y
624.0	3	18.35	Y	N
633.5	1	0.00	N	Y
635.5	2	0.00	N	Y
653.4	2	0.00	N	N
663.8	3	0.00	N	Y

* Degeneracy.
† Infrared intensity (Debye²/Å²/atomic mass unit).
‡ Infrared active.
§ Raman active.

experiment (Y$_2$O$_3$: a = 10.594 Å; YPO$_4$ a = 6.957 Å, c = 5.964 Å). Table 13 gives the thermodynamic properties of Y$_2$O$_3$, YPO$_4$, and P$_2$O$_5$. The calculated $\Delta E_{ox}^f(0)$ is, remarkably, within 1 kJ/mol

of the value calculated with VASP. The calculated corrections to obtain $\Delta H_{ox}^f(298.15)$ from $\Delta E_{ox}^f(0)$ from both the zero-point energy and the heat capacity are small, on the order of 1 kJ/mol or less. The main discrepancy with the empirical estimate is the calculated ZPE of the oxide. The calculated value for Y$_2$O$_3$ (33.5 kJ/mol) is higher than the value estimated from a force field parameterized against the measured vibrational spectra of A-type (La, Pr, Nd)$_2$O$_3$ given in Gopinath and Brown (1982). These are, of course, different structures. Calculated frequencies at q = (0,0,0) are given for YPO$_4$ and Y$_2$O$_3$ in Tables 14 and 15, and the phonon density of states for YPO$_4$(x) and C-Y$_2$O$_3$ are given in Figures 3 and 4. For YPO$_4$(x), there is good agreement between the vibrational frequencies and the Raman spectrum for xenotime reported in (http://www.ens-lyon.fr/LST/Raman). For Y$_2$O$_3$, there appear to be contributions at significantly higher frequencies than indicated in the measured spectrum (Repelin et al. 1995). It seems reasonable to conclude that the ΔZPE correction probably lies somewhere between 0 and +12 kJ/mol.
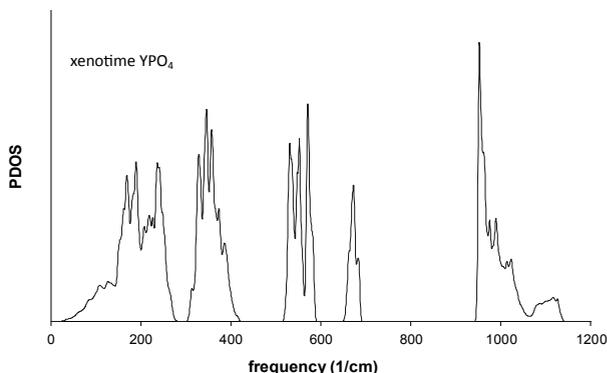
FIGURE 3. Phonon density of states computed for YPO$_4$-xenotime.

TABLE 15. Computed vibrational modes at q = (0,0,0) for YPO$_4$

ν (cm⁻¹)	g*	IR Int†	R‡	RM§
154.2	1	0.0	N	N
166.4	2	0.0	N	Y
190.3	1	0.0	N	Y
236.6	2	0.0	N	Y
237.7	2	10.1	Y	N
244.0	1	0.0	N	N
324.6	2	0.0	N	Y
339.2	1	0.0	N	Y
351.9	1	29.9	Y	N
352.9	1	0.0	N	Y
381.8	2	2.3	Y	N
418.0	1	0.0	N	N
518.9	1	0.0	N	Y
526.3	2	4.0	Y	N
577.5	1	0.0	N	N
584.8	2	0.0	N	Y
647.8	1	11.4	Y	N
669.2	1	0.0	N	Y
954.6	2	48.2	Y	N
957.6	1	0.0	N	N
971.7	1	0.0	N	Y
995.8	2	0.0	N	Y
1023.3	1	0.0	N	Y
1024.8	1	53.4	Y	N

* Degeneracy.
† Infrared intensity (Debye²/Å²/atomic mass unit).
‡ Infrared active.
§ Raman active.
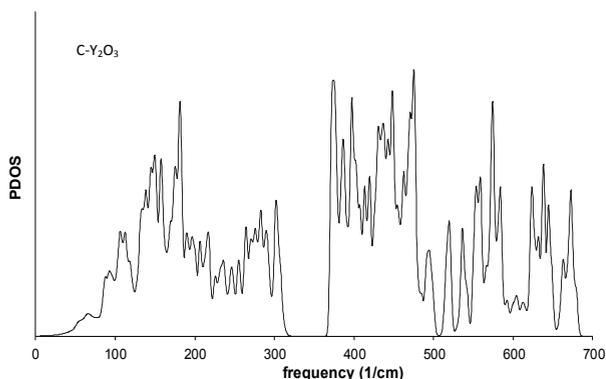
FIGURE 4. Phonon density of states computed for cubic Y_2O_3.
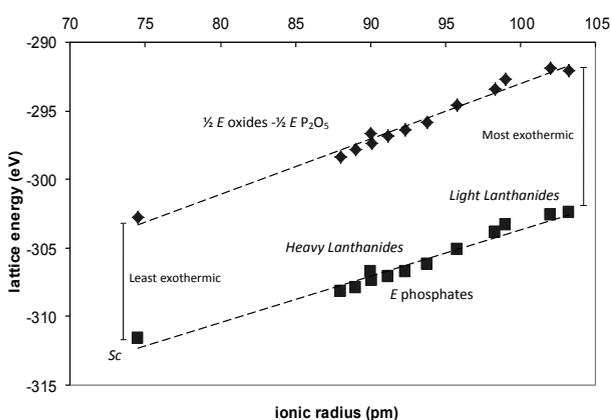
FIGURE 5. Electrostatic lattice energies E as a function of ionic radius for RE oxide and phosphate phases. The lattice energy of h-P_2O_5 has been added to the oxides and the sum multiplied by ½.

The physical origin of energetic trends

The overall trend of increasing ΔH_{ox}^r with ionic radius observed by Ushakov et al. (2002) and reproduced here using electronic structure calculations, is easy to understand. The electrostatic energies of the oxides and phosphate phases were computed in the ionic model assuming formal charges of +3 for the REE, –2 for oxygen, and +5 for phosphorous. Figure 5 shows the relationship between the electrostatic energy and the ionic radius for the oxide and phosphate phases. To make the comparison easier, the lattice energy of h-P_2O_5 has been added to the lattice energy of the oxide phases and the sum is multiplied by ½. The difference indicated in the figure is therefore the electrostatic energy of formation (this quantity is highly exothermic because it neglects short-range cation-anion repulsion). The reason for the observed trend is simply that, due to the localized charge on the oxide anions relative to the phosphate anions, the lattice energies of the oxide phases are a stronger function of ionic radius than the phosphates (compare the slopes of 0.82/2 eV/pm for the oxides and 0.34 eV/pm for the phosphates). In other words, the lattice energy becomes more negative for both phases as ionic radius decreases, but does so more rapidly for oxide phase than the phosphate phase because the anionic charge is more localized in the oxide. This type of trend governs the
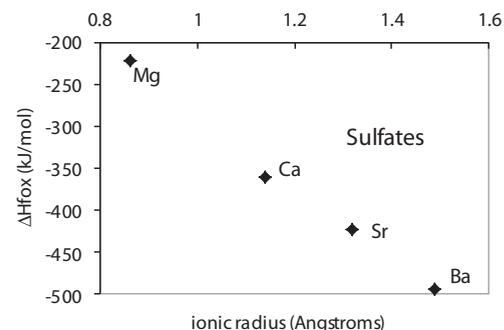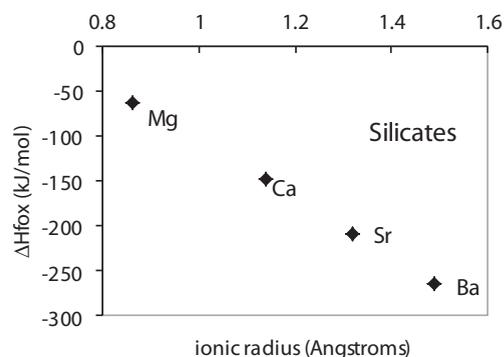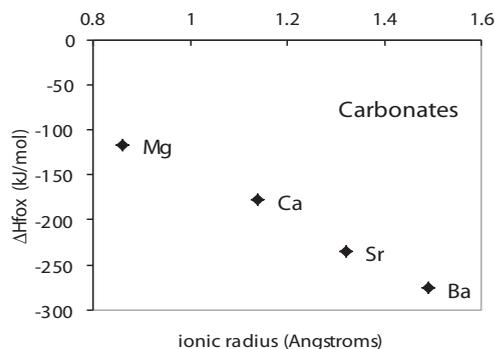
FIGURE 6. Correlation between measured enthalpies of formation from the oxides and ionic radius for carbonate (MCO_3), orthosilicate (M_2SiO_4), and sulfate(MSO_4) compounds with divalent anions. Experimental data are taken from the Materials Genome Reaction Calculator database (http://www.materialsproject.org).

enthalpies of formation of other oxyacid compounds as well, such as sulfates, carbonates, and silicates, as shown in Figure 6, with the measured ΔH_{ox}^r taken from the Materials Genome Project experimental database (http:// www.materialsproject.org).

Assessment of systematic error

An obvious approach to improving the accuracy of the electronic structure calculations is to account for the systematic error in a predictive manner. For example, it may be possible to scale the calculated ΔE_{ox}^r by some constant factor to estimate the

measured ΔH_{ox}^f. This factor would likely be material dependent; for example, there might be a scaling factor that will work for oxides, and a different one for sulfides. Additional accuracy may be obtained by introducing different scaling factors for different types of oxides (e.g., oxides sensu stricto, silicates, carbonates, sulfates), for example. Recent efforts in the construction of virtual databases of electronic structure calculations by the Materials Genome Project (MGP) (Jain et al. 2011) allow easy exploration of such questions. Table 9 gives the results of the Reaction Calculator program in MGP for the ΔE_{ox}^f of the RE orthophosphates calculated here. The details of these calculations are described on the MGP web site and Jain et al. (2011), but are much the same methods as used in this study. In fact, the RE phosphate ΔE_{ox}^f from MGP are very close to the calculations done in this study. Table 16 give enthalpies of formation from the oxides for alkaline earth carbonates, silicates, and sulfates calculated with the MGP. Omitting the $MgCO_3$, for which the MGP prediction seems anomalously low, an average scaling factor of 0.85 is obtained for $\Delta E_{ox\ calculated}^f / \Delta H_{ox\ measured}^f$. For the RE phosphates in Table 9, applying such a scaling factor to the MGP values (or the ones calculated here) gives nearly chemical accuracy (±4 kJ/mol) for most of the compounds. In the MGP database, $CePO_4$, $GdPO_4$, are not computed with the Ln_3 pseudopotentials. These compounds are also problematic for the calculations presented here, which use the Ln_3 pseudopotentials. In addition to these, $SmPO_4$ and $ScPO_4$ also give large errors, outside the bounds of chemical accuracy.

CONCLUDING REMARKS

Density functional electronic structure calculations have been carried out on Sc, Y, and RE orthophosphates and oxides, and h- and o'-P_2O_5 polymorphs to calculate the electronic enthalpies of formation $\Delta E_{ox}^f(0)$. Calculated enthalpies of formation are systematically less exothermic than measured $\Delta H_{ox}^f(298.15)$. $H(298.15) - H(0)$ corrections are estimated to be less than 1 kJ/mol. Empirical estimates for ZPE of orthophosphate and oxide phases are nearly independent of atomic number, and give a 0 to +12 kJ/mol correction to the $\Delta E_{ox}^f(0)$ (i.e., in the wrong direction; the reaction energies become less exothermic when ZPE is included). Ab initio calculation of the zero-point correction for formation of YPO_4, based on the computed vibrational spectrum of YPO_4 and Y_2O_3, gives ΔZPE and $\Delta[H(298.15) - H(0)]$ close to zero. Thus the origin of the discrepancy between the measured values of $\Delta H_{ox}^f(298.15)$ and calculated values of $\Delta E_{ox}^f(0)$ appears to be electronic in origin. Because similar errors are found for the alkaline earth carbonates, silicates, and sulfates, the errors do not result from the Ln_3 pseudopotentials or from errors in the calculated energy of the P_2O_5 reference phase. Because the PBE functional is likely to underestimate the charge localization, it seems further unlikely that using hybrid functionals will fix the problem; they are likely to give more "ionic" electronic structures which should favor the oxides over the phosphates, making the enthalpies of formation even less exothermic. These observations, taken together, would suggest that improvement in the absolute value of the calculated $\Delta E_{ox}^f(0)$ could require going beyond density functional theory, e.g., quantum Monte Carlo (see Kolorenc and Mitas 2011).

Nevertheless, near-chemical accuracy (±10 kJ/mol) for most

TABLE 16. Energies calculated from the MGP Reaction Calculator vs. measured enthalpies taken from MGP database, and the ratios of these numbers

	$\Delta E_{ox}^f(0)$ kJ/mol	ΔH_{ox}^f kJ/mol	$\Delta E_{ox}^f(0)/\Delta H_{ox}^f$
$MgCO_3$	−81	−117	0.69
$CaCO_3$	−148	−178	0.83
$SrCO_3$	−198	−235	0.84
$BaCO_3$	−238	−276	0.86
$MgSO_4$	−196	−222	0.88
$CaSO_4$	−299	−361	0.83
$SrSO_4$	−351	−423	0.83
$BaSO_4$	−414	−495	0.84
Mg_2SiO_4	−53	−63	0.84
Ca_2SiO_4	−127	−147	0.86
Sr_2SiO_4	−179	−208	0.86
Ba_2SiO_4	−236	−265	0.89

of the compounds can be obtained by dividing the calculated $\Delta E_{ox}^f(0)$ by 0.85; a value taken from the average scaling factor between measured ΔH_{ox}^f and ΔE_{ox}^f calculated from the Materials Genome Project database on alkaline earth carbonates, silicates, and sulfates, obtained with methods similar to those used here.

Finally, a qualitative understanding of the observed correlation between atomic number and heat of formation results from the lanthanide contraction and the localized charge on the oxide anion relative to the phosphate anion and can be reproduced from the simplest ionic model, without input from any deep aspects of the quantum mechanics.

REFERENCES CITED

Adelstein, N., Mun, B.S., Ray, H.L., Ross, P.N. Jr., Neaton, J.B., and De Jonghe, L.C. (2011) Structure and electronic properties of cerium orthophosphate: Theory and experiment. Physical Review B, 83, 205104.

Andon, R.J.L.,Counsell, J.F., McKerrell, H., and Martin, J.F. (1963) Thermodynamic properties of phosphorous compounds. 1. Entropy of phosphorous pentoxide. Transactions of the Faraday Society, 59, 2702–2705.

Baldinozzi, G., Berar, J., and Calvarin, G. (1998) Rietveld refinement of two-phase Zr-doped Y_2O_3. Materials Science Forum, 278, 680–685.

Bartos, A., Lieb, K.P., Uhrmacher, M., and Wiarda, D. (1993) Refinement of atomic positions in bixbyite oxides using perturbed angular-correlation spectroscopy. Acta Crystallographica, B49, 165–169.

Bloechl, P.E. (1994) Projector augmented-wave method. Physical Review B, 50, 17953.

Boucherle, J.X. and Schweizer, J. (1975) Refinement of Nd_2O_3 structure and determination of neutron-scattering length of neodymium. Acta Crystallographica, B31, 2745–2746.

Boulesteix, C., Pardo, B., Caro, P.E., Gasgnier, M., and la Blanchetais, C.H. (1971) Etude de couches minces de sesquioxyde de samarium type B par microscopie et diffraction électroniques. Acta Crystallographica, B27, 216–219.

Clark, S.J., Segall, M.D., Pickard, C.J., Hasnip, P.J., Probert, M.J., Refson, K., and Payne, M.C. (2005) First-principles methods using CASTEP. Zeitschrift für Kristallographie, 220, 567–570.

Cruickshank, D.W.J. (1964) Refinements of structures containing bonds between Si, P, S, or Cl+O or N V. P_4O_{10}. Acta Crystallographica, 17, 677–679.

Da Silva, J.L. (2007) Stability of the Ce_2O_3 phases: a DFT+U investigation. Physical Review B, 76, 193108.

Dudarev, S.L., Botton, G.A., Savrasov, S.Y., Szotek, Y., Temmerman, W.M., and Sutton, A.P. (1998) Electronic structure and elastic properties of strongly correlated metal oxides from first principles: LSDA+U, SIC-LSDA and EELS study of UO_2 and NiO. Physica status solidi (a), 166, 429–443.

Fabris, S., de Gironcoli, S., Baroni, S., Vicario, G., and Balducci, G. (2005) Taming multiple valency with density functionals: A case of defective ceria. Physical Review B, 71, 041102.

Fert, A. (1962) Structure de quelques oxydes de terres rares. Bulletin de la Societe Francaise de Mineralogie et de Cristallographie, 85, 267–270.

Gavrichev, K.S., Gorbunov, V.E., Golushina, L.N., Nikiforova, G.E., Totrova, G.A., and Shaplygin, I.S. (1993) Calorimetry and thermodynamic properties of Y_2O_3 in 14–300 K temperature range. Zhurnal Fizichyeskoi Khimi, 67, 1731–1733 (in Russian).

Gavrichev, K.S., Smirnova, N.N., Gurevich, V.M., Danilov, V.P., Tyurin, A.V., Ryu-

min, M.A., and Komissarova, L.N. (2006) Heat capacity and thermodynamic functions of LuPO$_4$ in the range 0–320 K. Thermochimica Acta, 448, 63–65.

Gavrichev, K.S., Ryumin, M.A., Tyurin, A.V., Gurevich, V.M., and Komissarova, L.N. (2008) Refined heat capacity of LaPO$_4$ in the temperature range 0–1600 K. Thermochimica Acta, 474, 47–51.

Gavrichev, K.S., Ryumin, M.A., Tyurin, A.V., Gurevich, V.M., and Komissarova, L.N. (2010a) Heat capacity and thermodynamic functions of pretulite ScPO$_4$(c) at 0–1600 K. Geochemistry International, 48, 390–397.

Gavrichev, K.S., Ryumin, M.A., Tyurin, A.V., Gurevich, V.M., and Komissarova, L.N. (2010b) Heat capacity and thermodynamic functions of xenotime YPO$_4$(c) at 0–1600 K. Geochemistry International, 48, 932–939.

Gilliam, S.J., Kirby, S.J., Merrow, C.N., Zeroka, D., Banerjee, A., and Jensen, J.O. (2003) Raman spectroscopy of rhombohedral P$_4$O$_{10}$. Journal of Physical Chemistry B, 107, 2892–2896.

Goldstein, H.W., Neilson, E.F., Walsh, P.N., and White, D. (1959) The heat capacities of yttrium oxide (Y$_2$O$_3$), lanthanum oxide (La$_2$O$_3$), and neodymium oxide (Nd$_2$O$_3$) from 16 to 300 degrees K. Journal of Physical Chemistry, 63, 1445–1449.

Gopinath, C.R. and Brown, I.D. (1982) Normal coordinate analysis of the Raman and infrared vibrations of the alpha phases of La$_2$O$_3$, Pr$_2$O$_3$, Nd$_2$O$_3$, La$_2$O$_2$S, YB$_2$O$_2$S. Journal of Raman Spectroscopy, 12, 278–280.

Greenwood, N.N. and Earnshaw A. (1985) Chemistry of the Elements. Butterworth Heinemann, Oxford.

Greis, O., Ziel, R., Breidenstein, B., Haase, A., and Petzel, T. (1994) The crystal-structure of the low-temperature A-type modification of Pr$_2$O$_3$ from X-ray powder and electron single crystal diffraction. Journal of Alloys and Compounds, 216, 255–258.

Gruber, J.B., Justice, B.H., Westrum, E.F., and Zandi, B. (2002) Revisiting the thermophysical properties of the A-type hexagonal lanthanide sesquioxides between temperatures of 5 K and 1000 K. Journal of Chemical Thermodynamics, 34, 457–473.

Hase, W. (1963) Neutronographische bestimmung der kristallstrukturparameter von Dy$_2$O$_3$, Tm$_2$O$_3$, und alpha-Mn$_2$O$_3$. Physica Status Solidi, 3, 446–449.

Hirosaki, N., Ogata, S., and Kocer, C.J. (2003) Ab initio calculation of the crystal structure of the lanthanide Ln$_2$O$_3$ sesquioxides. Alloys and Compounds, 351, 31–34.

Jain, A., Hautier, G., Moore, C.J., Ong, S.P., Fischer, C.C., Mueller, T., Persson, K.A., and Ceder, G. (2011) A high-throughput infrastructure for density functional theory calculations. Computational Materials Science, 50, 2295–2310.

Justice, B.H. and Westrum, E.F. (1963) Thermophysical properties of the lanthanide oxides. 2. Heat capacities, thermodynamic properties and some energy levels of samarium(III), gadolinium(III), and ytterbium(III) oxides from 10 to 350 degrees K. Journal of Physical Chemistry, 67, 345–351.

Justice, B.H., Westrum, E.F., Chang, E., and Radebaug, R. (1969) Thermophysical properties of the lanthanide oxides. 4. Heat capacities and thermodynamic properties of thulium(III) and lutetium(III) oxides. Electronic energy levels of several lanthanide (III) ions. Journal of Physical Chemistry, 73, 333–340.

Knop, O. and Hartley, J.M. (1968) Refinement of the crystal structure of scandium oxide. Canadian Journal of Chemistry, 46, 1446–1450.

Koehler, W.C. and Wollan, E.O. (1953) Neutron-diffraction study of the structure of the A-form of the rare earth sesquioxides. Acta Crystallographica, 6, 741–742.

Kolorenc, J. and Mitas, L. (2011) Applications of quantum Monte Carlo methods in condensed systems. Reports on Progress in Physics, 74, 1–28.

Kresse, G. and Furthmuller, J. (1996) Efficiency of ab-initio total energy calculations for metals and semiconductors using a plane-wave basis set. Computational Materials Science, 6, 15–50.

Kresse, G. and Hafner, J. (1993) Ab initio molecular dynamics for liquid-metals Physical Review B, 47, 558–561.

Kresse, G. and Joubert, D. (1999) From ultrasoft pseudopotentials to the projector augmented-wave method. Physical Review B, 59, 1758–1775.

Kuemmerle, E.A. and Heger, G.J. (1999) The structures of C-Ce$_2$O$_3$+delta, Ce$_7$O$_{12}$, and Ce$_{11}$O$_{20}$. Journal of Solid State Chemistry, 147, 485–500.

Lin, J.S., Qteish, A., Payne, M.C., and Heine, V. (1993) Optimized and transferable nonlocal separable ab initio pseudopotentials. Physical Review B, 47, 4174–4180.

Loschen, C., Carrasco, J., Neyman, K.M., and Illas, F. (2007) First-principles LDA plus U and GGA plus U study of cerium oxides: Dependence on the effective U parameter. Physical Review B, 75, 035115.

Milligan, W.O., Mullica, D.F., Beall, G.W., and Boatner, L.A. (1982) Structural investigations of YPO$_4$, ScPO$_4$, and LuPO$_4$. Inorganica Chimica Acta, 60, 39–43.

Ni, Y., Hughes, J.M., and Mariano, A.N. (1995) Crystal chemistry of the monazite and xenotime structures. American Mineralogist, 80, 21–26.

Pedone, A., Malavasi, G., Menziani, M.C., Cormack, A.N., and Segre, U. (2006) A new self-consistent empirical interatomic potential model for oxides, silicates, and silica-based glasses. Journal of Physical Chemistry B, 110, 11780–11795.

Perdew, J.P., Burke, K., and Ernzerhof, M. (1996) Generalized gradient approximation made simple. Physical Review Letters, 77, 3865–3868.

Refson, K., Clark, S.J., and Tulip, P.R. (2006) Variational density-functional perturbation theory for dielectrics and lattice dynamics. Physical Review B, 73, 155114.

Repelin, Y., Proust, C., Husson, E., and Beny, J.M. (1995) Vibrational spectroscopy of the C-form of yttrium sesquioxide. Journal of Solid State Chemistry, 118, 163–169.

Rustad, J.R. (2011) Vibrational spectrum and low-temperature heat capacity of rhombohedral P$_4$O$_{10}$. arXiv:1106.5824v1[cond-mat.mtrl-sci].

Saiki, A., Ishizawa, N., Mizutani, N., and Kato, M. (1985) Structural change of rare earth sesquioxides Yb$_2$O$_3$ and Er$_2$O$_3$ as a function of temperature. Journal of the Ceramic Society of Japan, 93, 649–654.

Schiller, G. Die Kristallstrukturen von Ce$_2$O$_3$ (1985) (A-Form), LiCeO$_2$ und CeF$_3$—Ein Beitrag zur Kristallchemie des dreiwertigen Cers. Dissertation Universitaet Karlsruhe.

Silva, E.N., Ayala, A.P., Guedes, I., Paschoal, C.W.A., Moriera, R.L., Loong, C.-K., and Boatner, L. (2006) Vibrational spectra of monazite-type rare-earth orthophosphates. Optical Materials, 29, 224–230.

Stachel, D., Svoboda, I., and Fuess, H. (1995) Phosphorous pentoxide at 233 K. Acta Crystallographica, C51, 1049–1050.

Ushakov, S.V., Helean, K.B., and Navrotsky, A. (2002) Thermochemistry of rare-earth orthophosphates. Journal of Materials Research, 16, 2623–2633.

Weller, W.W. and King, E.G. (1963) Report Invest No. 6245, p. 1–6. U.S. Bureau of Mines, Washington, D.C.

Westrum, E.F. and Justice, B.H. (1963) Thermophysical properties of the lanthanide oxides. 2. Heat capacities, thermodynamic properties and some energy levels of dysprosium(III), holmium(III), and erbium(III) oxides. Journal of Physical Chemistry, 67, 659–665.

Westrum, E.F. (1985) Schottky contributions in chemical thermodynamics. Journal of Thermal Analysis and Calorimetry, 30, 1209–1215.

Wu, B., Zinkevich, M., Aldinger, F., Wen, D., and Chen, L. (2007) Ab initio study on the structure and phase transition of A- and B-type rare-earth sesquioxides Ln$_2$O$_3$(Ln=La-Lu, Y, and Sc) based on density functional theory. Journal of Solid State Chemistry, 180, 3280–3287.

Zhang, F.X., Lang, M., Wang, J.W., Becker, U., and Ewing, R.C. (2008) Structural phase transitions of cubic Gd$_2$O$_3$ at high pressures. Physical Review B, 78, 064114.